Calcif Tissue Int (1993) 52:199–204

Calcified Tissue International

Geometric Variables from DXA of the Radius Predict Forearm Fracture Load *In Vitro*

Elizabeth R. Myers, Aaron T. Hecker, Daniel S. Rooks, John A. Hipp, and Wilson C. Hayes

Orthopaedic Biomechanics Laboratory, Department of Orthopaedic Surgery, Charles A. Dana Research Institute, Beth Israel Hospital, Boston, Massachusetts 02215, USA

Received July 20, 1992, and in revised form September 24, 1992

Summary. The purpose of this investigation was to determine the cross-sectional geometry of the radius in female and male cadaveric specimens using dual-energy X-ray absorptiometry (DXA), to measure the accuracy of this technique compared with a digitizing procedure, and to measure the correlation between these DXA-based geometric variables and the load required to produce a forearm fracture. Paired intact forearms were scanned at a distal site and at a site approximately 30% of the forearm length from the distal end. The cross-sectional area and the moments of inertia of two sections at 10 and 30% of the forearm length were computed from the X-ray attenuation data. One member of each pair was then sectioned at the 30% location, which is mostly cortical bone, and the section was traced on a digitizing pad. The other forearm was loaded to failure in a servohydraulic materials test system. The DXA-based area and moment of inertia at 30% correlated significantly with the digitized results ($r^2 = 0.93$ for area; $r^2 = 0.95$ for moment; $P < 0.001$). The conventional bone mineral density from DXA did not associate significantly with failure load, but the minimum moment of inertia and the cross-sectional area at 10% correlated in a strong and significant manner with the forearm fracture force ($r^2 = 0.67$ for area; $r^2 = 0.66$ for moment; $P < 0.001$). The determination of radial bone cross-sectional geometry, therefore, should have better discriminatory capabilities than bone mineral density in studies of bone fragility and fracture risk.

Key words: Dual-energy X-ray absorptiometry – Colles' fracture – Bone mineral density – Distal radius – Forearm fracture.

The high incidence of fractures of the hip [1], spine [2], and distal radius [3] in the elderly is thought to be the result of age-related bone loss and concomitant reductions in bone strength. As a consequence, many noninvasive techniques have been developed to assess age-related bone loss [4–6]. Surprisingly few studies, however, have assessed the accuracy of these techniques for predicting the failure load in cadaveric specimens of the hip [7–12], vertebral body [13, 14], or forearm [15–18]. Moreover, the resulting relationships between density and failure load are obscured by differences in densitometric variables and in failure test configurations. To understand the relationship between noninvasive techniques and bone fracture loads, regional bone mineral assessments should be correlated with the loads required to produce typical age-related fracture patterns.

One of the most attractive sites for noninvasive bone densitometry is the forearm; it is accessible and the radius and ulna are surrounded by small amounts of soft tissue and fat. The most commonly used noninvasive methods for measuring radial bone mass are single photon absorptiometry [19] and, more recently, dual-energy X-ray absorptiometry (DXA) [20–22]. DXA measurements are taken in an anteroposterior direction using a X-ray source, and bone mineral content (BMC) is determined by subtracting the attenuation of the X-rays in soft tissue from the attenuation in bone plus soft tissue [5]. Areal bone mineral "density" (BMD) is calculated as the BMC divided by the frontal projected area of the bone, and consequently it is not exactly equal to true volumetric bone density [23]. The accuracy of DXA has been measured in cadaveric lumbar specimens, with a very strong correlation of BMC against ash weight but with a relatively large regression error for projected area by DXA against volume of bone [24].

Osteopenia of the radius assessed by bone densitometry has been found to associate significantly with increased risk or incidence of fracture [25–41]. There are two potential problems, however, with the use of BMD as a clinical predictor of fracture risk: BMD does not represent true volumetric bone density [23, 24]; and the failure load of a bone such as the radius depends not only on the bone density and architecture but also on the cross-sectional geometry of the bone [42]. Previously we found that BMD determined by single photon absorptiometry (SPA) did not correlate with the failure force of the distal radius in cadaveric specimens, whereas cross-sectional geometric variables and BMC did correlate strongly and significantly with force [15]. We hypothesized that the same would be true for DXA properties, so we adapted our multiple-angle SPA methods [15], based in part on the technique of Martin and Burr [16], for use with a DXA densitometer to calculate the cross-sectional geometry of the distal radius.

We asked the following questions: (1) What is the accuracy of the multiple-angle method of computing cross-sectional geometry of the radius from DXA? (2) Do the geometric variables of the radius vary between males and females and between a distal measuring site versus a location in the diaphysis? and (3) Does the cross-sectional geometry of the distal radius provide a stronger predictor of the force required to cause a forearm fracture *ex vivo* over standard radial BMD? We found that BMD did not correlate significantly with failure load, but that the minimum moment of inertia and the cross-sectional area from DXA correlated in a strong and significant manner with the force required to create a forearm fracture. The availability of methods that

Offprint requests to: E. R. Myers

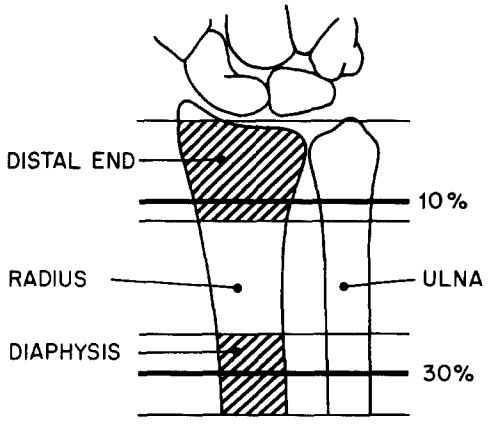

Fig. 1. Diagram of the bones of the forearm illustrating the two sites for DXA scanning: (1) the distal end of the radius starting from the distal styloid process of the ulna and extending proximally to 12.5% of the total forearm length; and (2) 2 cm of the diaphysis of the radius centered on the 30% mark. Two scan lines at 10 and 30% of the total forearm length were extracted for cross-sectional analysis.

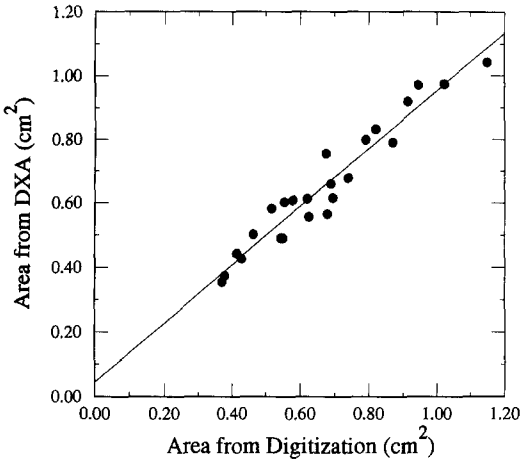

Fig. 2. Cross-sectional area of the radius at 30% as measured by digitization versus DXA. The correlation coefficient between the two methods was r = 0.97 ($P < 0.001$, n = 24).

account for both geometric and densitometric effects thus could be expected to provide stronger local predictors of fracture risk at the distal radius and stronger predictors of fracture risk at remote sites than the use of bone density alone.

Materials and Methods

Twenty-five pairs of cadaveric arms were obtained fresh-frozen from the Harvard Anatomic Gifts Program. The specimens came from elderly donors; the mean age was 74 years with a standard deviation of 9 years. Eighteen (72%) of the donors were female and 7 (28%) were male. The specimens were stored at −20°C until testing. One specimen was noted by X-ray to have had a previous fracture and was excluded from the analysis.

Specimens were defrosted and wrapped in cellophane to avoid dehydration of the soft tissues. The total forearm length was measured from the styloid process of the ulna to the olecranon. A special holding device, described previously for use with SPA [15], was used to position the forearm in a dual-energy X-ray absorptiometer (QDR-1000, Hologic Inc., Waltham, MA). The fingers of each specimen were wrapped around a grip on the holding device that allowed rotation of the bones of the forearm about the longitudinal axis. The radius of each forearm was scanned at two locations using the high resolution setting of the QDR-1000 and a pencil beam from a collimator with a diameter of 0.6 mm. The point distance at the high resolution setting was 0.127 mm. Both the distal end of the radius and the radial diaphysis were scanned, and scan lines were extracted from the raw data for cross-sectional analysis corresponding to 10 and 30% of the total forearm length (Fig. 1). At each location, separate scans were taken at 0° (fully pronated position), 20°, and 40° from full pronation. The X-ray attenuation curve at each angle was used to compute the bone cross-sectional area and cross-sectional moment of inertia about the axis parallel to the X-ray beam [15, 16]. The geometric data at the three angles were then used to determine the principal moments of inertia (I_{max} and I_{min}) using standard formulations for rotation of reference axes [43]. Cross-sectional properties were determined for both the right and left radius from each of the forearm pairs.

The accuracy of this method was evaluated by selecting at random one forearm from each pair for a digitizing procedure. The soft tissues were cleaned from the radius and ulna, and the bones were embedded in polyurethane foam [15, 44]. Care was taken to mark and orient the radius and ulna in a fully pronated position before embedding. After the foam hardened, the bones were sectioned with a band saw at the same 30% location as described above. The 30% location was chosen because it is composed predominantly of cortical bone [45] and could be used with the digitizing procedure to give a "gold standard" to compare with the cross-sectional properties derived from DXA. Slides were taken of each section and projected onto a Talos digitizing pad (Talos RP-622, Scottsdale, AZ). A single operator traced the boundaries of each radial section, and the cross-sectional properties were computed using the SLICE software program [46].

The remaining forearm from each pair of specimens was loaded in a failure test to simulate the configuration of the arm during a fall onto the outstretched hand. Each forearm was cut 15 cm proximal to the wrist joint, and soft tissue was then removed from the proximal 3 inches of the radius and ulna. The cleaned radius and ulna were embedded in an aluminum container using polyester resin (Dynotron/Bondo Corporation, Atlanta, GA). The aluminum mold was clamped to the hydraulic piston of an Instron model 1331 servohydraulic material testing system (Instron, Canton, MA). The intact hand was placed against a horizontal upper stage with 75° dorsiflexion of the wrist and 10° internal rotation [15]. A ramp displacement of 25 mm/second was applied to each mounted specimen, and the force-displacement data were recorded using LabTech Notebook (Laboratory Technologies, Wilmington, MA).

To analyze our data, linear bivariate correlations between the geometric bone properties derived from DXA attenuation curves and maximum force in the failure test were examined. The BMC and areal BMD of the radius were also correlated with the failure force. Variations in bone properties with gender and location were tested by analysis of variance with gender as a grouping factor and location as a trial factor. We also examined the potential predictors of failure force in a multiple stepwise regression with backward and forward stepping. The variables entered into the model were I_{min}, cross-sectional area, and BMD. These variables were chosen because they could all be potential independent predictors of the failure force under combined compression and bending conditions. Data analysis was carried out with BMDP programs 2V and 2R [47].

Results

In a region of the radius that is mostly cortical bone, there was a very strong linear correlation ($r^2 = 0.93$, $P < 0.001$) between cross-sectional area determined noninvasively from DXA and cross-sectional area determined destructively from digitization (Fig. 2). The cross-sectional moment derived from DXA about the anteroposterior centroidal axis versus that derived from digitization also resulted in a strong and significant linear correlation ($r^2 = 0.95$, $P < 0.001$, Fig. 3).

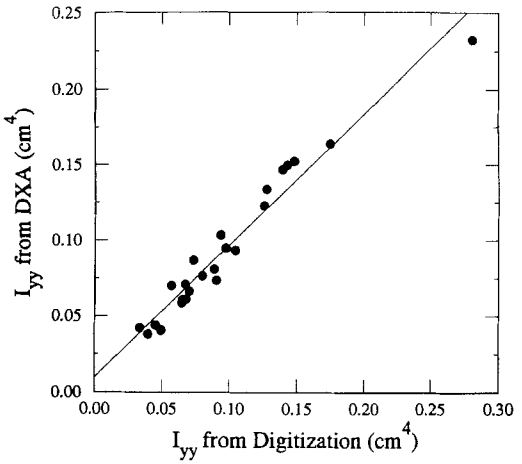

Fig. 3. The cross-sectional moment of inertia about the anteroposterior axis (I_{yy}) of the 30% radial section as measured by digitization versus DXA. The correlation coefficient between the two methods was r = 0.98 ($P < 0.001$, n = 24).

The mean values for BMD did not differ between samples from elderly men compared with elderly women ($P = 0.65$, Table 1). The radii from elderly males did have larger bone width, cross-sectional area, and moments of inertia than the radii from females (Table 1). The BMD of the radial shaft centered at 30% of the total forearm length was significantly higher than the BMD of the distal site ($P < 0.001$). The geometric properties of the 30% section were all smaller than the geometric properties at the 10% section ($P < 0.001$).

Radiographs taken after the failure test revealed Colles' fracture patterns [48] in 19 of the 24 forearm specimens. Two specimens had fractures of the radial shaft at the level of the embedding medium, two had ulnar fractures, and one did not fail. The mean failure force for the 19 specimens with Colles' fracture patterns was 1780 ± 650 Newtons (N), and the force was significantly higher in males than females ($P < 0.01$, Table 1). Failure force values for all specimens are displayed in Figure 4 against the minimum moment of inertia at the 10% cross section. The line in Figure 4 is for the specimens that showed Colles' fracture patterns only. Significant bivariate correlations between failure force and bone properties of the distal radius were found for bone width, cross-sectional area, I_{max}, and I_{min} (Table 2). There were no significant correlations between failure force and BMC or BMD of the distal site (Table 2).

In the stepwise regression model, two variables associated significantly with failure force: I_{min} and BMD. The addition of BMD significantly increased the multiple correlation coefficient over the value for just I_{min} alone, with a resultant multiple correlation coefficient of $R = 0.88$ ($R^2 = 0.78$). The reduction in the residuals is illustrated in Figure 5; there is less spread for the values from the linear multiple fit than for the observed values. The significance of I_{min} and BMD held under both forward and backward stepping.

Discussion

Dual-energy X-ray absorptiometry at multiple angles in the radius provided an accurate determination of the cross-sectional geometry. In addition, the cross-sectional area and principal moments of inertia assessed by DXA were larger in males than in females. BMD of the distal radius did not correlate significantly with the force required for forearm fracture in cadaveric specimens except in a multiple regression model. Cross-sectional area and I_{min} gave the strongest bivariate correlations with fracture force and could thus be used in future studies of fracture risk to predict the structural strength of the distal radius.

Studies of Colles' fracture in adults have observed low levels of radial BMD and BMC in fracture subjects compared with controls [28–31, 33, 34]. These investigations often enroll 50 to over 100 subjects and find the mean decrease in the BMD of Colles' patients to be only about 12% [28]. Our *in vitro* results for 19 specimens showed no significant linear bivariate correlations between BMD or BMC of the distal radius and forearm fracture load. This apparent discrepancy between the clinical results and the *in vitro* results could be due to several possible reasons. First, our study design did not have the power to detect a significant but weak correlation between two variables. We would have needed approximately 80 cadaveric specimens to have a 90% chance of detecting a significant correlation coefficient of 0.35 at a significance level of 0.05. It is possible that a bivariate correlation was not detected with only 19 specimens showing fracture patterns typical of Colles' fracture. Second, BMD did turn out to account for a significant portion of the variance in fracture force once I_{min} was included in a multiple linear regression model. The association between BMD and force was positive and significant. This result indicates that though geometry of the radius may dominate the fracture load in this elderly sample of cadaveric forearms, BMD also associates significantly with fracture load. Third, our laboratory loading conditions in the failure test were controlled and simplified when compared against the many external loading conditions that cause forearm fracture in clinical surveys. Any conclusions about the relationship of geometry and density to forearm strength apply only to this specific loading configuration, although we were careful to include only specimens that showed radiographic evidence of Colles' fracture patterns. Fourth, we did not have the software package available that calculates BMD for a precise ultradistal site in the radius such as that used in clinical studies. We used the BMD of the distal end as illustrated in Figure 1. The error introduced by using a scan window that is larger than that dictated by the commercial software is unknown and could be investigated in future studies. However, the values for BMD did overlap the range of values for measurements made at the ultradistal site in younger samples *in vivo* [21, 22].

The fracture force values measured in our experiment were similar to those measured by Frykman [48] using human cadaveric specimens and a test configuration similar to ours. Frykman found that the mean fracture force in male specimens was 2770 N and the force in females was 1920 N. The mean age in Frykman's study (65 years) was slightly younger than the mean age for our specimens (74 years). The mean force measured in this study (1780 N) was less than the mean value we found in a previous series of experiments (3390 N) [15], but the ranges overlapped (500–3020 N versus 2100–5500 N). There were more females specimens in the current study than in our previous study, which could explain some of the difference.

Significant correlations have been measured previously between failure load of intact or excised specimens of radius or ulna and BMC by SPA [15, 18, 49] and X-ray absorptiometry [17]. In our previous work with SPA [15], we found that BMC was proportional to the cross-sectional area of the radius at a single scan line and that it correlated significantly with the force in the forearm fracture test. With the rectilin-

Table 1. Properties of the radius in males and females[a]

Property	Location	Males	Females	Significance[b]
BMC (g)	Distal end	1.62 (0.95)	1.72 (1.10)	NS
	Diaphysis	1.23 (0.60)	1.12 (0.60)	
BMD (g/cm^2)	Distal end	0.232 (0.057)	0.289 (0.150)	NS
	Diaphysis	0.449 (0.213)	0.462 (0.227)	
Cross-sectional area (cm^2)	10%	1.00 (0.176)	0.597 (0.152)	<0.001
	30%	0.886 (0.087)	0.568 (0.124)	
Bone width (cm)	10%	2.52 (0.47)	1.94 (0.28)	0.001
	30%	1.59 (0.12)	1.44 (0.16)	
I_{min} (cm^4)	10%	0.343 (0.104)	0.144 (0.056)	<0.001
	30%	0.111 (0.057)	0.058 (0.034)	
I_{max} (cm^4)	10%	0.461 (0.152)	0.201 (0.069)	<0.001
	30%	0.191 (0.035)	0.086 (0.023)	
Maximum force (N)		2370 (420)	1580 (600)	<0.01

[a] Mean (SD)
[b] Significance of difference with gender

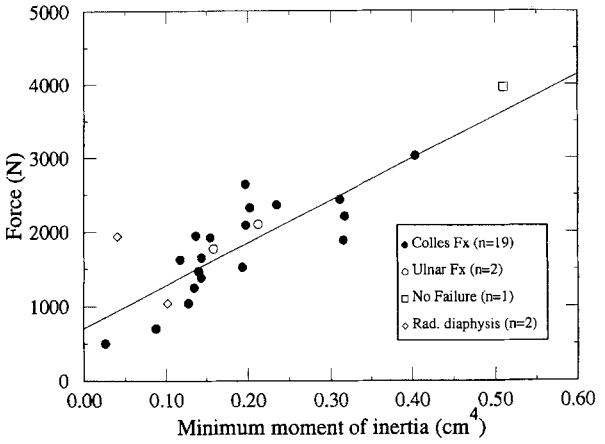

Fig. 4. Minimum moment of inertia (I_{min}) of the 10% section as determined by DXA versus the failure load in the forearm fracture test. Nineteen specimens showed patterns of Colles' fracture by radiograph, two failed by fracture of the ulna only, one did not fail, and two had fractures at the level of the embedding medium. The correlation coefficient between I_{min} and the failure force for the 19 specimens with Colles' fracture patterns was r = 0.81 (r^2 = 0.66, P < 0.001, n = 19), and the equation of the line was Force = 5720 I_{min} + 710 N. The standard error of the estimate was 390 N.

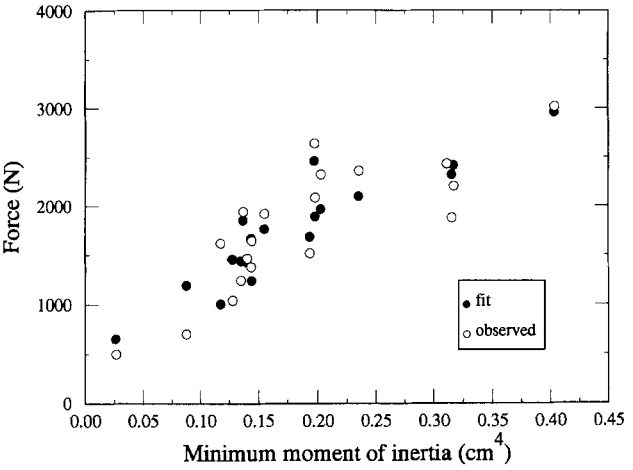

Fig. 5. Results of the multiple linear regression. The open circles are the values that were observed for the 19 specimens with patterns of Colles' fracture. The closed circles are the values from the multiple linear regression. The model was Force = 6140 I_{min} + 1910 BMD + 50 N, with a multiple correlation coefficient of R = 0.88 (R^2 = 0.78, F = 28.8, n = 19). The standard error of the estimate was 320 N. The inclusion of BMD in the model after I_{min} resulted in a significant reduction in the residuals (change in R^2 = 0.12, F = 9.0).

Table 2. Correlation coefficients between forearm failure load and radial bone properties at the distal end

Property	r	r^2	Significance
Bone width	0.50	0.25	0.03
Cross-sectional area	0.82	0.67	<0.001
I_{max}	0.62	0.38	0.005
I_{min}	0.81	0.66	<0.001
BMC	0.35	0.12	NS
BMD	0.26	0.07	NS

ear scan utilized by DXA, however, BMC is the sum in two directions of the mineral pathlength and therefore should be proportional to the volume of bone mineral in the scan window. BMC assessed by DXA did not associate significantly with *in vitro* failure load, however, which was surprising considering that it is a measure of the amount of bone mineral in the distal section. It seems that measuring the amount of bone mineral (BMC) or the areal density (BMD) in a segment of the radius does not offer the same predictive capacity for force as measuring the geometry at a single scan line at the 10% location.

Bone mineral measurements are potentially useful in clinical observational studies and in clinical trials if the regional bone measurement provides an assessment of fracture strength. Among the variables measured for the distal radius, the strongest linear relationship with the forearm fracture force was with cross-sectional geometric variables such as the area and I_{min}. For this reason, the determination of radial bone cross-sectional geometry could have better discriminatory capabilities than BMD in studies of bone fragility and fracture risk. We plan in the future to determine the correlation between these new DXA-based variables of the forearm and failure loads at other sites in the body. We will also investigate the measurement of these DXA variables in both the hip and the spine.

Acknowledgments. This study was supported by a grant from the

National Institutes of Health (R01 AR40321) and by the Maurice E. Mueller Professorship in Biomechanics at Harvard Medical School (WCH). The authors would like to thank Jeanine Goodwin for her assistance in manuscript preparation, Michael Harrington for data management and programming, and Marienne Moro for assistance with the digitizing protocol.

References

1. Melton LJ III (1988) Epidemiology of fractures. In: Riggs BL, Melton LJ III (eds) Osteoporosis: etiology, diagnosis, and management. New York, Raven Press, pp 133–154
2. Melton LJ, Kan SH, Frye MA, Wahner HW, O'Fallen WM, Riggs BL (1989) Epidemiology of vertebral fractures in women. Am J Epidemiol 129:1000–1011
3. Owen RA, Melton LJ III, Johnson KA, Ilstrup DM, Riggs BL (1982) Incidence of Colles' fracture in a North American community. Am J Public Health 72:605–607
4. Genant HK, Block JE, Steiger P, Glueer CC, Ettinger B, Harris ST (1989) Appropriate use of bone densitometry. Radiology 170:817–822
5. Mazess RB (1990) Bone densitometry of the axial skeleton. Orthop Clin N Am 21:51–63
6. Wahner HW (1989) Measurements of bone mass and bone density. Endocrinol Metab Clin N Am 18:995–1013
7. Lotz JC, Hayes WC (1990) Estimates of hip fracture risk from falls using quantitative computed tomography. J Bone Joint Surg [Am] 72:689–700
8. Myers ER, Hecker AT, Rooks DS, Hayes WC (1992) Correlations of the failure load of the femur with densitometric and geometric properties from QDR. Trans 38th ORS, 17:115
9. Beck TJ, Ruff CB, Warden KE, Scott WW, Rao GU (1990) Predicting femoral neck strength from bone mineral data. Invest Radiol 25:6–18
10. Sartoris DJ, Sommer FG, Kosek J, Gies A, Carter D (1985) Dual-energy projection radiography in the evaluation of femoral neck strength, density, and mineralization. Invest Radiol 20: 476–485
11. Dalen N, Hellstrom LG, Jacobson B (1976) Bone mineral content and mechanical strength of the femoral neck. Acta Orthop Scand 47:503–508
12. Leichter I, Margulies JY, Weinreb A, Mizrahi J, Robin GC, Conforty B, Makin M, Bloch B (1982) The relationship between bone density, mineral content, and mechanical strength in the femoral neck. Clin Orthop 163:272–281
13. McBroom RJ, Hayes WC, Edwards WT, Goldberg RP, White AA III (1985) Prediction of vertebral body compressive fracture using quantitative computed tomography. J Bone Joint Surg [AM] 67:1206–1214
14. Mosekilde L, Bentzen SM, Ortoft G, Jorgensen J (1989) The predictive value of quantitative computed tomography for vertebral body compressive strength and ash density. Bone 10:465–470
15. Myers ER, Sebeny EA, Hecker AT, Corcoran TA, Hipp JA, Greenspan SL, Hayes WC (1991) Correlations between photon absorption properties and failure load of the distal radius in vitro. Calcif Tissue Int 49:292–297
16. Martin BR, Burr DB (1984) Non-invasive measurement of long bone cross-sectional moment of inertia by photon absorptiometry. J Biomech 17:195–201
17. Horsman A, Currey JD (1983) Estimation of mechanical properties of the distal radius from bone mineral content and cortical width. Clin Orthop 176:298–304
18. Jurist JM, Foltz AS (1977) Human ulnar bending stiffness, mineral content, geometry and strength. J Biomech 10:455–459
19. Cameron JR, Sorenson JA (1963) Measurement of bone mineral in vivo: an improved method. Science 142:230–232
20. Weinstein RS, New KD, Sappington LJ (1991) Dual-energy x-ray absorptiometry versus single photon absorptiometry of the radius. Calcif Tissue Int 49:313–316
21. Larcos G, Wahner HW (1991) An evaluation of forearm bone mineral measurement with dual-energy x-ray absorptiometry. J Nucl Med 32:2101–2106
22. Overton TR, Wheeler GD (1992) Bone mass measurements in the distal forearm using dual-energy x-ray absorptiometry and x-ray computed tomography: a longitudinal, in vivo comparative study. J Bone Miner Res 7:375–381
23. Carter DR, Bouxsein ML, Marcus R (1992) New approaches for interpreting projected bone densitometry data. J Bone Miner Res 7:137–144
24. Ho CP, Kim RW, Schaffler MB, Sartoris DJ (1990) Accuracy of dual-energy radiographic absorptiometry of the lumbar spine: cadaver study. Radiology 176:171–173
25. Overgaard K, Hansen MA, Riis BJ, Christiansen C (1992) Discriminatory ability of bone mass measurements (SPA and DEXA) for fractures in elderly post-menopausal women. Calcif Tissue Int 50:30–35
26. Hui SL, Slemenda CW, Johnston CC Jr (1989) Baseline measurement of bone mass predicts fracture in white women. Ann Int Med 111:355–361
27. Hui SL, Slemenda CW, Johnston CC (1988) Age and bone mass as predictors of fracture in a prospective study. J Clin Invest 81:1804–1809
28. Eastell R, Wahner HW, O'Fallen M, Amadio PC, Melton LJ III, Riggs BL (1989) Unequal decrease in bone density of lumbar spine and ultradistal radius in Colles' and vertebral fracture syndromes. J Clin Invest 83:168–174
29. Hesp R, Klenerman L, Page L (1984) Decreased radial bone mass in Colles' fracture. Acta Orthop Scand 55:573–575
30. Nilsson BE, Westlin NE (1974) The bone mineral content in the forearm of women with Colles' fracture. Acta Orthop Scand 45:836–844
31. Harma M, Karjalainen P (1986) Trabecular osteopenia in Colles' fracture. Acta Orthop Scand 57:38–40
32. Gardsell P, Johnell O, Nilsson BE (1989) Predicting fractures in women by using forearm bone densitometry. Calcif Tissue Int 44:235–242
33. Lester GE, Anderson JJB, Tylavsky FA, Sutton WR, Stinnett SS, DeMasi RA, Talmage RV (1990) Update on the use of distal radial bone density measurements in prediction of hip and Colles' fracture risk. J Orthop Res 8:220–226
34. Eastell R, Riggs BL, Wahner HW, O'Fallon WM, Amadio PC, Melton LJ (1989) Colles' fracture and bone density of the ultradistal radius. J Bone Miner Res 4:607–613
35. Smith DA, Hosie CJ, Deacon AD, Hamblen DL (1990) Quantitative x-ray computed tomography of the radius in normal subjects and osteoporotic patients. Br J Radiol 63:776–782
36. Smith DA, Johnston CC, Yu P-L (1972) In vivo measurement of bone mass. Its use in demineralized states such as osteoporosis. JAMA 219:325–329
37. Grubb SA, Jacobson PC, Awbrey BJ, McCartney WH, Vincent LM, Talmage RV (1984) Bone density in osteopenic women: a modified distal radius density measurement procedure to develop an "at risk" value for use in screening women. J Orthop Res 2:322–327
38. Ross PD, Davis JW, Epstein RS, Wasnich RD (1991) Preexisting fractures and bone mass predict vertebral fracture incidence in women. Ann Intern Med 114:919–923
39. Cummings SR, Black DM, Nevitt MC, Browner WS, Cauley JA, Genant HK, Mascioli SR, Scott JC (1990) Appendicular bone density and age predict hip fracture in women. JAMA 263:665–668
40. Voort J, Taconis WK, Schaik CL, Silberbusch J (1990) The relationship between densitometry of the radius and vertebral fractures. Neth J Med 37:53–57
41. Black DM, Cummings SR, Genant HK, Nevitt MC, Palermo L, Browner W (1992) Axial and appendicular bone density predict fractures in older women. J Bone Miner Res 7:633–638
42. Hayes WC, Gerhart TN (1985) Biomechanics of bone: applications for assessment of bone strength. In: Peck WA (ed) Bone and mineral research, annual III. Elsevier Science Publishers, Amsterdam, pp 259–294
43. Shames IH (1967) Engineering mechanics: statics and dynamics. Prentice-Hall, Englewood Cliffs
44. Ruff CB, Hayes WC (1984) Bone mineral content in the lower

limb: relationship to cross-sectional geometry. J Bone Joint Surg [Am] 66:1024–1031
45. Schlenker RA, VonSeggen WW (1976) The distribution of cortical and trabecular bone mass along the lengths of the radius and ulna and the implications for in vivo bone mass measurements. Calcif Tissue Int 20:41–52
46. Nagurka ML, Hayes WC (1980) Technical note: an interactive graphics package for calculating cross-sectional properties of complex shapes. J Biomech 13:59–64
47. Dixon WJ (1990) BMDP statistical software manual. University of California Press, Berkeley
48. Frykman G (1967) Fracture of the distal radius including sequelae-shoulder-hand-finger syndrome: disturbance in the distal radio-ulnar joint and impairment of nerve function. A clinical and experimental study. Acta Orthop Scand 108:1–153
49. Spadaro JA, Werner FW, Brenner RA, Fay LA, Fortino MD (1992) The contribution of cortical bone to osteopenic distal radius strength. Trans 38th ORS 17:113